

# Constraining Astrophysical Neutrino Flavor Composition from Leptonic Unitarity

Xun-Jie Xu,<sup>a</sup> Hong-Jian He,<sup>a</sup> Werner Rodejohann<sup>b</sup>

<sup>a</sup>Institute of Modern Physics and Center for High Energy Physics,  
Tsinghua University, Beijing 100084, China.

Center for High Energy Physics, Peking University, Beijing 100871, China.

<sup>b</sup>Max-Planck-Institut für Kernphysik, Postfach 103980, D-69029 Heidelberg, Germany.

E-mail: [xunjie.xu@gmail.com](mailto:xunjie.xu@gmail.com), [hjhe@tsinghua.edu.cn](mailto:hjhe@tsinghua.edu.cn),  
[werner.rodejohann@mpi-hd.mpg.de](mailto:werner.rodejohann@mpi-hd.mpg.de)

## Abstract.

The recent IceCube observation of ultra-high-energy astrophysical neutrinos has begun the era of neutrino astronomy. In this work, using the unitarity of leptonic mixing matrix, we derive nontrivial unitarity constraints on the flavor composition of astrophysical neutrinos detected by IceCube. Applying leptonic unitarity triangles, we deduce these unitarity bounds from geometrical conditions, such as triangular inequalities. These new bounds generally hold for three flavor neutrinos, and are independent of any experimental input or the pattern of leptonic mixing. We apply our unitarity bounds to derive general constraints on the flavor compositions for three types of astrophysical neutrino sources (and their general mixture), and compare them with the IceCube measurements. Furthermore, we prove that for any sources without  $\nu_\tau$  neutrinos, a detected  $\nu_\mu$  flux ratio  $< 1/4$  will require the initial flavor composition with more  $\nu_e$  neutrinos than  $\nu_\mu$  neutrinos.

**Keywords:** Neutrino properties, Ultra high energy photons and neutrinos, Neutrino theory  
JCAP (2014) Final Version, [arXiv:1407.3736].

**ArXiv ePrint:** [1407.3736](https://arxiv.org/abs/1407.3736)

---

## Contents

<b>1</b>	<b>Introduction</b>	<b>2</b>
<b>2</b>	<b>Connecting Astrophysical Neutrinos to Leptonic Unitarity Triangle</b>	<b>3</b>
<b>3</b>	<b>Unitarity Constraints on Flavor Transitions of Astrophysical Neutrinos</b>	<b>5</b>
<b>4</b>	<b>Unitarity Constraints on Flavor Ratios of Astrophysical Neutrinos</b>	<b>11</b>
4.1	Pion Sources with Flavor Ratio (1:2:0)	11
4.2	Muon-Damped Sources with Flavor Ratio (0:1:0)	15
4.3	Neutron Beam Sources with Flavor Ratio (1:0:0)	17
4.4	Mixed Sources with Flavor Ratio ( $\eta:1-\eta:0$ )	18
<b>5</b>	<b>Conclusions</b>	<b>21</b>
	<b>References</b>	<b>23</b>

---

## 1 Introduction

With the recent IceCube observation [1, 2] of ultra-high-energy astrophysical neutrinos, the era of neutrino astronomy has finally begun. The IceCube collaboration has detected a flux of ultra-high-energy cosmic neutrinos (TeV–PeV), which have  $5.7\sigma$  significance above the atmospheric neutrino backgrounds [2] and thus point to their extraterrestrial origin. Contrary to charged particles which would deflect in magnetic fields in space, such astrophysical neutrinos are expected to point straight back to their sources. The potential impact of understanding these neutrinos ranges from acceleration mechanisms of cosmic rays to fundamental particle physics [3]. Studying the flavor composition of astrophysical neutrinos provides an invaluable tool for exploring these issues. The developments of neutrino telescopes (such as IceCube and alike) [1, 2, 4] in recent years have stimulated extensive studies [5, 6] on the flavor ratios. Given these dedicated studies, it is desirable to find general constraints on the cosmic neutrino flavor compositions.

In this work, we will derive such general constraints by imposing the unitarity of leptonic mixing matrix [7], because the leptonic mixing modifies the neutrino flavor ratios during their trip from source to detector. The general bounds we obtain do not depend on the neutrino mixing parameters or any experimental input. Especially, we will use leptonic unitarity triangles (LUTs) [8][9] as geometrical means to derive such universal constraints, which turn out to be highly nontrivial. The unitarity bounds are important, because any violation of

these bounds would call for new physics, such as active-sterile neutrino mixing, neutrino decays, pseudo-Dirac neutrinos, or other exotic effects [10].

We will then apply our general unitarity bounds to the commonly considered sources of ultra-high-energy astrophysical neutrinos, including Pion Sources, Muon-Damped Sources, and Neutron Beam Sources. We compare these bounds with the IceCube measurement [2] and the current global fit of neutrino oscillations [11, 12]. Our unitarity bounds can put general constraints on the emerging flavor ratios from the IceCube data, independent of specific pattern of leptonic mixing. Furthermore, we will prove that for any astrophysical sources without  $\nu_\tau$  neutrinos, if the detected  $\nu_\mu$  neutrinos have a flux ratio  $T < 1/4$ , then the source must generate more  $\nu_e$  neutrinos than  $\nu_\mu$  neutrinos. These results demonstrate the importance of our general unitarity constraints. In passing, aspects of the IceCube events were also discussed recently in [13, 15].

The paper is organized as follows. In Section 2, we will connect the neutrino flavor ratios to the geometrical parameters of the LUTs. Then, we will use our geometrical formulation to analyze the general unitarity constraints on the flavor transition probabilities in Section 3. We apply these constraints to derive nontrivial bounds on the flavor ratios for typical astrophysical neutrino sources, and compare them with the IceCube data in Section 4. Finally, we conclude in Section 5.

## 2 Connecting Astrophysical Neutrinos to Leptonic Unitarity Triangle

The leptonic mixing in charged currents is described by the  $3 \times 3$  unitary matrix  $U$  of Pontecorvo-Maki-Nakagawa-Sakata (PMNS) [7]. The orthogonality between the rows (columns) of  $U$  forms the LUTs. Following the conventions of our recent study [8], we define the lengths of the three sides of the LUTs,

$$(a, b, c) \equiv (|U_{\ell 1}U_{\ell' 1}|, |U_{\ell 2}U_{\ell' 2}|, |U_{\ell 3}U_{\ell' 3}|), \quad (2.1)$$

where the subscripts  $\ell$  and  $\ell'$  stand for the three flavors ( $\ell \neq \ell'$ ). For each length parameter among  $(a, b, c)$ , we have suppressed the subscripts  $\ell\ell'$  for simplicity. The flavor transition probability for astrophysical neutrinos  $\nu_\ell \rightarrow \nu_{\ell'}$  is given by

$$P_{\ell \rightarrow \ell'} = \sum_j |U_{\ell j}U_{\ell' j}|^2, \quad (2.2)$$

which does not contain the oscillation terms since such terms are simply averaged out due to the very large  $L/E$  of astrophysical neutrinos. From this, we can further express the transition probability (2.2) in terms of the LUT parameters,

$$P_{\ell \rightarrow \ell'} = a^2 + b^2 + c^2. \quad (2.3)$$

For  $\ell \neq \ell'$ , we can classify the flavor appearance probability  $P_{\ell \rightarrow \ell'}$  into three cases,

$$\begin{aligned} X &= a_{\mu\tau}^2 + b_{\mu\tau}^2 + c_{\mu\tau}^2, \\ Y &= a_{\tau e}^2 + b_{\tau e}^2 + c_{\tau e}^2, \\ Z &= a_{e\mu}^2 + b_{e\mu}^2 + c_{e\mu}^2. \end{aligned} \tag{2.4}$$

Hence, we can rewrite (2.2) in a matrix form,

$$\mathbb{P} = \begin{pmatrix} 1-Y-Z & Z & Y \\ Z & 1-X-Z & X \\ Y & X & 1-X-Y \end{pmatrix}, \tag{2.5}$$

where the diagonal elements correspond to survival probability,

$$P_{\ell \rightarrow \ell} = 1 - \sum_{\ell' (\neq \ell)} P_{\ell \rightarrow \ell'}, \tag{2.6}$$

because the full transition probability equals one. For an initial flux from a remote astrophysical neutrino source, let us denote its initial flavor compositions as  $(\Phi_{e0}, \Phi_{\mu0}, \Phi_{\tau0})$ . Thus, the detected neutrino flux (after traveling an astronomical distance) can be computed in the matrix form,

$$(\Phi_e, \Phi_\mu, \Phi_\tau)^T \propto \mathbb{P} (\Phi_{e0}, \Phi_{\mu0}, \Phi_{\tau0})^T. \tag{2.7}$$

For neutrino telescopes such as IceCube, the high energy muon neutrinos are in principle distinctive from  $\nu_e$  and  $\nu_\tau$  signals as they produce clear muon tracks in the detector. Hence, the flavor ratio  $\Phi_\mu/\Phi_{\text{tot}}$  is a good observable for these experiments [1, 2, 4], where  $\Phi_{\text{tot}} = \Phi_e + \Phi_\mu + \Phi_\tau$ . The other possibly measurable ratio is  $\Phi_e/\Phi_{\text{tot}}$  if the electron neutrino signals can be recognized in the near future. (The flavor ratio  $\Phi_\tau/\Phi_{\text{tot}}$  for tau neutrinos can be deduced from the other two ratios.) The  $\nu_\mu$  and  $\nu_e$  flavor ratios are conventionally defined as

$$T = \frac{\Phi_\mu}{\Phi_{\text{tot}}}, \quad S = \frac{\Phi_e}{\Phi_{\text{tot}}}, \tag{2.8}$$

and thus  $\Phi_\tau/\Phi_{\text{tot}} = 1 - T - S$ . In the literature, sometimes another flavor ratio  $R \equiv \Phi_e/\Phi_\tau$  is introduced to replace  $S$ . But the description by  $(T, S)$  is equivalent to that of  $(T, R)$  because

$$S = (1-T) \frac{R}{1+R}, \quad R = \frac{S}{1-T-S}. \tag{2.9}$$

Inspecting the formulas (2.4), we find that under the exchange  $\nu_e \leftrightarrow \nu_\mu$ , the transition probabilities  $(X, Y, Z)$  change as follows:  $X \leftrightarrow Y$  and  $Z \leftrightarrow Z$ . This also corresponds to

the exchanges of the first and second rows (columns) of the matrix  $\mathbb{P}$  in Eq. (2.5). With Eqs. (2.7) and (2.8), we further infer  $T \leftrightarrow S$  under the same exchange of  $\nu_e \leftrightarrow \nu_\mu$ .

Typically, let us consider three types of commonly studied neutrino sources, i.e., Pion Sources ( $\pi$ S), Muon-Damped Sources ( $\mu$ DS), and Neutron Beam Sources ( $n$ BS).

- The  $\pi$ S sources produce neutrinos from pion decays,  $\pi \rightarrow \mu + \nu_\mu \rightarrow e + \nu_e + 2\nu_\mu$ , where we do not distinguish the notations between particles and anti-particles for simplicity. Hence, the initial flavor composition is  $(1 : 2 : 0)$ . From Eq. (2.7), the  $\nu_\mu$  and  $\nu_e$  flux ratios in this case are given by

$$T = \frac{1}{3}(2 - 2X - Z), \quad S = \frac{1}{3}(1 - Y + Z). \quad (2.10)$$

- The  $\mu$ DS sources produce muon neutrinos in  $\pi \rightarrow \mu + \nu_\mu$ , where the damped muons lose energy so that the neutrino flux produced from their decays is depleted at energies of interest. Hence, the initial flavor composition is  $(0 : 1 : 0)$ . From Eq. (2.7), we have the  $\nu_\mu$  and  $\nu_e$  flux ratios,

$$T = 1 - X - Z, \quad S = Z. \quad (2.11)$$

- The Neutron Beam Sources ( $n$ BS) produce electron neutrinos in beta decay of neutrons. Thus, its initial flavor composition is  $(1 : 0 : 0)$ . From Eq. (2.7), the  $\nu_\mu$  and  $\nu_e$  flux ratios are given by

$$T = Z, \quad S = 1 - Z - Y. \quad (2.12)$$

For the current experiments, which source the detected high-energy astrophysical neutrinos originate from is uncertain. Nevertheless, we note that if all three types of sources are involved, the initial neutrino flux would contain no  $\nu_\tau$  neutrinos. Let us consider a general source with mixture [5] from all three types of sources above. In this case, the initial flavor composition can be written as,  $(\eta : 1 - \eta : 0)$ , with the parameter  $\eta \in [0, 1]$ . Hence, in the general case, we have  $T$  and  $S$  flux ratios depending on  $\eta$ ,

$$T = \eta Z + (1 - \eta)(1 - X - Z), \quad (2.13a)$$

$$S = \eta(1 - Z - Y) + (1 - \eta)Z. \quad (2.13b)$$

### 3 Unitarity Constraints on Flavor Transitions of Astrophysical Neutrinos

The leptonic mixing matrix of PMNS [7] is unitary,  $UU^\dagger = I$ , which imposes two kinds of constraints on the row vectors  $(U_{\ell 1}, U_{\ell 2}, U_{\ell 3})$ . These include, (i) the normalization conditions,

$$|U_{\ell 1}|^2 + |U_{\ell 2}|^2 + |U_{\ell 3}|^2 = 1, \quad (3.1)$$

and (ii) the orthogonal conditions,

$$U_{\ell_1}^* U_{\ell_1} + U_{\ell_2}^* U_{\ell_2} + U_{\ell_3}^* U_{\ell_3} = 0, \quad (\ell \neq \ell'). \quad (3.2)$$

The second constraint (3.2) implies the closure of the corresponding unitarity triangle, since the three complex numbers can be represented by three vectors in the complex plane and the zero sum makes them form a closed triangle. In terms of the lengths of three sides  $(a, b, c)$ , the closure imposes nontrivial triangular inequalities, stating that the sum of the lengths of any two sides is larger than the remaining side,

$$a + b \geq c, \quad a + c \geq b, \quad b + c \geq a, \quad (3.3)$$

where the equality sign corresponds to the collapse of the triangle into a line. Another equivalent statement is that the difference between the lengths of any two sides is smaller than the remaining side, because  $a - b \leq c$  is just  $b + c \geq a$ , and so on. Hence, Eq. (3.3) is sufficient to describe the triangular closure constraints.

The geometrical meaning of the first constraint (3.1) does not appear so obvious, but in fact it restricts the length scale of the three sides. Let us define the notations,  $(a_1, b_1, c_1) \equiv (|U_{\ell_1}|, |U_{\ell_2}|, |U_{\ell_3}|)$  and  $(a_2, b_2, c_2) \equiv (|U_{\ell'_1}|, |U_{\ell'_2}|, |U_{\ell'_3}|)$ . Thus, we can express the three sides,  $(a, b, c) = (a_1 a_2, b_1 b_2, c_1 c_2)$ . Using the Cauchy–Schwarz inequality<sup>1</sup>, we deduce

$$(a_1 a_2 + b_1 b_2 + c_1 c_2)^2 \leq (a_1^2 + b_1^2 + c_1^2)(a_2^2 + b_2^2 + c_2^2) \leq 1. \quad (3.4)$$

From this, we deduce that the perimeter of the triangle (the sum of its three sides) cannot exceed one,

$$a + b + c \leq 1. \quad (3.5)$$

With this, we can further derive an upper bound on the Jarlskog invariant  $J = \text{Im}\{U_{\ell'_j} U_{\ell_j}^* U_{\ell_k} U_{\ell'_k}^*\}$ , with  $\ell \neq \ell'$  and  $j \neq k$  [16], fully from geometry. The Euclidean geometry tells us that a shape with fixed perimeter reaches the maximal area when it is a circle, and for a triangle with fixed perimeter, its maximal area is realized when it is an equilateral triangle, with  $a = b = c$  and the corresponding area  $S_{\text{max}} = \sqrt{3}a^2/4$ . (Intuitively, the equilateral triangle in some sense looks like a circle more than any other triangles.) Since the Jarlskog invariant equals twice the area of the LUT, the maximum  $|J|$  is given by the equilateral unitarity

---

<sup>1</sup> The Cauchy–Schwarz inequality is well-known in mathematics, which states,  $(x_1 y_1 + x_2 y_2 + \dots + x_n y_n)^2 \leq (x_1^2 + x_2^2 + \dots + x_n^2)(y_1^2 + y_2^2 + \dots + y_n^2)$ . Another key inequality we use in this work is that the arithmetical mean is smaller than the corresponding quadratic mean,  $(x_1 + x_2 + \dots + x_n)/n \leq \sqrt{(x_1^2 + x_2^2 + \dots + x_n^2)/n}$ . For more detail, see for instance, G. H. Hardy, J. E. Littlewood, and G. Polya, *Inequalities*, 1952, Cambridge University Press.

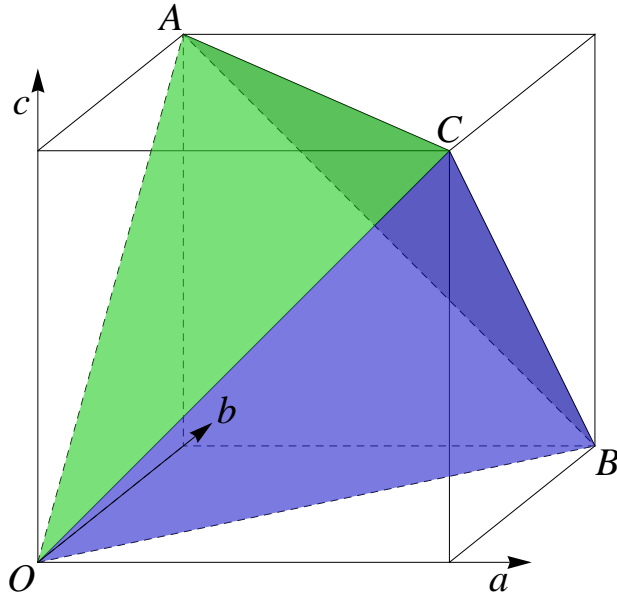


**Figure 1.** Unitarity constraints on the lengths of sides for any leptonic unitarity triangle,  $(a, b, c)$ . Each side of the cube has length equal  $1/2$ , and thus  $(a, b, c)$  cannot be larger than  $1/2$ . The equations of planes  $ABC$ ,  $OAC$ ,  $OBC$  and  $OAB$  are  $a + b + c = 1$ ,  $a + b = c$ ,  $b + c = a$ , and  $c + a = b$ , respectively. The unitarity requires  $(a, b, c)$  to be a point inside the tetrahedron  $OABC$ .

triangle,  $|J|_{\max} = \sqrt{3}a^2/2$  with  $a = 1/3$ . Hence, without using any parameter from the conventional PMNS matrix, we can derive the general geometrical upper bound on  $|J|$ ,

$$|J| \leq \frac{1}{6\sqrt{3}}. \quad (3.6)$$

Even though the condition (3.5) appears quite different from (3.3), geometrically they are very similar as Fig. 1 illustrates. Each side of the cube in Fig. 1 has length equal  $1/2$ . Hence, the equation of the plane  $ABC$  is,  $a + b + c = 1$ . The inequality (3.5) is derived from the normalization condition (3.1), and it requires that the allowed region should be on one side of the plane  $ABC$ . The other planes of the tetrahedron are planes  $OAC$ ,  $OBC$  and  $OAB$ , corresponding to  $a + b = c$ ,  $b + c = a$  and  $c + a = b$ , respectively. These planes make a tetrahedron with each side of length  $1/\sqrt{2}$ . The inequalities (3.5) and (3.3) only require that  $(a, b, c)$  is a point inside the tetrahedron. Thus, we can immediately infer the upper bound on the length of each side for any LUT,

$$a, b, c \leq \frac{1}{2}. \quad (3.7)$$

Next, we would ask: what are the unitarity bounds on the averaged transition probabilities  $(X, Y, Z)$  defined in Eq. (2.4)? Here, we can deduce and visualize the bounds geometrically. Consider a sphere with its center at  $(0, 0, 0)$ . The sphere retains some of the

allowed points  $(a, b, c)$  on it, and has intersections with the tetrahedron. It should have a radius no larger than  $1/\sqrt{2}$ . Hence, we deduce

$$a^2 + b^2 + c^2 \leq \frac{1}{2}. \quad (3.8)$$

Using Eq. (2.4), we infer the nontrivial upper bound,

$$X, Y, Z \leq \frac{1}{2}. \quad (3.9)$$

We stress that we derived these constraints only from the unitarity of the PMNS matrix, without any experimental input. This means that for astrophysical neutrinos (or any neutrinos traveling with a large enough  $L/E$ ), the flavor appearance probability for any two flavors ( $\ell \rightarrow \ell'$ ) cannot exceed  $1/2$ ,

$$P_{\ell \rightarrow \ell'} \leq \frac{1}{2}. \quad (3.10)$$

Another nontrivial result we will prove is that the survival probability is bounded from below, always no smaller than  $1/3$ ,

$$P_{\ell \rightarrow \ell} \geq \frac{1}{3}. \quad (3.11)$$

The survival probability  $P_{\ell \rightarrow \ell}$  is just the diagonal elements of the matrix (2.5). To prove (3.11), we first choose  $\ell = e$  for definiteness,  $P_{e \rightarrow e} = 1 - Y - Z$ . Note that  $Y + Z = (a_{\tau e}^2 + b_{\tau e}^2 + c_{\tau e}^2) + (a_{e\mu}^2 + b_{e\mu}^2 + c_{e\mu}^2)$ , where the terms  $a_{\tau e}^2 + a_{e\mu}^2$ , for instance, can be written as

$$\begin{aligned} a_{\tau e}^2 + a_{e\mu}^2 &= |U_{e1}|^2 (|U_{\mu 1}|^2 + |U_{\tau 1}|^2) \\ &= |U_{e1}|^2 (1 - |U_{e1}|^2). \end{aligned} \quad (3.12)$$

We can derive similar formulas for  $b_{\tau e}^2 + b_{e\mu}^2$  and  $c_{\tau e}^2 + c_{e\mu}^2$ . With these, we arrive at

$$\begin{aligned} Y + Z &= \sum_{j=1}^3 |U_{ej}|^2 (1 - |U_{ej}|^2) = 1 - \sum_{j=1}^3 |U_{ej}|^4 \\ &\leq 1 - \frac{1}{3} \left( \sum_{j=1}^3 |U_{ej}|^2 \right)^2 \leq \frac{2}{3}. \end{aligned} \quad (3.13)$$

This leads to  $P_{e \rightarrow e} \geq \frac{1}{3}$ . The first inequality in the second line of Eq. (3.13) is based on the fact that the arithmetic mean of several real numbers is always smaller than their quadratic mean (cf. footnote-1). Likewise, we can prove that  $X + Y$  and  $Z + X$  obey the same inequality,

$$X + Y, Y + Z, Z + X \leq \frac{2}{3}. \quad (3.14)$$

With these, we complete the proof of the lower bound (3.11) on the survival probability.



Furthermore, we will prove the following nontrivial inequalities,

$$Y+2Z, Z+2X, X+2Y \leq \frac{25}{24}, \quad (3.15a)$$

$$2Y+Z, 2Z+X, 2X+Y \leq \frac{25}{24}. \quad (3.15b)$$

We present the proof as follows. Without losing generality, we take  $Y+2Z$  for instance. Let us inspect the difference,

$$\begin{aligned} G &\equiv (Y+2Z) - 1 \\ &= \sum_j |U_{ej}|^2 (2|U_{\mu j}|^2 + |U_{\tau j}|^2 - 1) \\ &= \sum_j |U_{ej}|^2 (|U_{\mu j}|^2 - |U_{ej}|^2). \end{aligned} \quad (3.16)$$

Our proof will be achieved so long as we demonstrate the maximum value,  $G_{\max} = \frac{1}{24}$ . Since  $G$  only depends on the first two rows of the PMNS matrix, we can generally write the squared elements in a matrix form,

$$|U_{\ell\ell'}|^2 \equiv \begin{pmatrix} x & y & 1-x-y \\ z & w & 1-z-w \\ \times & \times & \times \end{pmatrix}, \quad (3.17)$$

where “ $\times$ ” denote elements of no interest here. The quantity  $G$  is a function of  $(x, y, z, w)$ , which may be regarded as equivalents to the four independent parameters of the PMNS matrix. Using the notation (3.17), we can rewrite the function  $G$ ,

$$G = xz + yw + (1-x-y)(1-z-w) - [x^2 + y^2 + (1-x-y)^2]. \quad (3.18)$$

If we overlook the boundary of parameter space, we would naively seek the maximum by solving  $\partial_x G = \partial_y G = \partial_z G = \partial_w G = 0$ . This gives a unique solution,  $x = y = z = w = \frac{1}{3}$ , which results in  $G = 0$ . But, as can be readily checked, this solution is actually a saddle point, rather than the maximum. This implies that the maximum of  $G$  should be on the boundary, since this saddle point is the only place where the first derivatives of  $G$  vanish. Hence, we will inspect the maximum of  $G$  on the boundary of parameter space.

The relevant parameter space is where  $(x, y, z, w)$  satisfies (i)  $x, y, z, w \geq 0$  and  $x + y, z + w \leq 1$ , and (ii) the triangle inequalities  $a + b \geq c, a + c \geq b, b + c \geq a$ , where  $a = \sqrt{xz}$ ,  $b = \sqrt{yw}$ , and  $c = \sqrt{(1-x-y)(1-z-w)}$ . Any  $(x, y, z, w)$  satisfying these two conditions can realize a unitary PMNS matrix. When we are on the boundary of the condition (i), then the first two rows of (3.17) must contain one zero element. We will prove that only when the second row has a zero element,  $G$  realizes its global maximum. In this

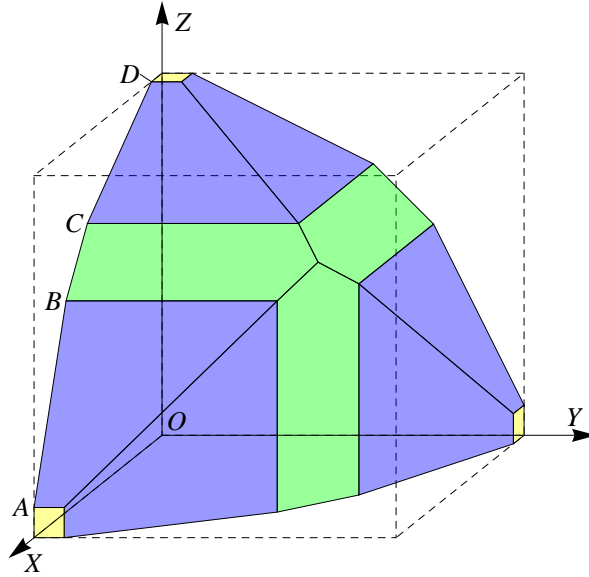


**Figure 2.** Unitarity constraints on the averaged neutrino transition probabilities  $(X, Y, Z)$ . Each side of the cube has length equal to  $\frac{1}{2}$ . The conditions (3.9) confine the  $(X, Y, Z)$  space into the cube. The equations for the green planes are  $(X+Y, Y+Z, Z+X) = \frac{2}{3}$ , while for the blue planes they are  $(2X+Y, 2X+Z, 2Y+Z, 2Y+X, 2Z+X, 2Z+Y) = \frac{25}{24}$ . The unitarity of the PMNS matrix requires  $(X, Y, Z)$  to be a point inside the region bounded by the colored surfaces.

case, without losing generality, we set the third element of this row be zero, i.e.,  $1 - z - w = 0$ , then we can resolve  $\partial_{x,y,z} G|_{w=1-z} = 0$ . We find the solution,  $(x, y, z) = (\frac{5}{12}, \frac{5}{12}, \frac{1}{2})$  and  $w = 1 - z = \frac{1}{2}$ . This gives the maximum,

$$G_{\max} = \frac{1}{24}. \quad (3.19)$$

Next, we will prove that the other cases either have no extremum or have the extremum not as a global maximum. If the maximum of  $G$  is on the boundary of the condition (i), but with the zero element in the first row of (3.17), we may set  $1 - x - y = 0$  without losing generality. In this case, we find that the extremum equation  $\partial_{x,z,w} G|_{x=1-y} = 0$  has no solution by direct calculation.

If the maximum is instead on the boundary of the condition (ii), we have one of the triangle inequalities saturated. Since it is not on the boundary of the condition (i), all the elements of the two rows are non-zero, which means that  $(a, b, c)$  are all non-zero. Hence, only one of the triangle inequalities can be saturated. Without losing generality, we consider the situation  $a + b = c$ . This is a hypersurface,  $F(x, y, z, w) = 0$ , in the parameter space where

$$F = (a + b)^2 - c^2 = xz + yw + 2\sqrt{xyzw} - (1 - x - y)(1 - z - w). \quad (3.20)$$

The extremum point can be found by the method of Lagrange multipliers. This is to solve  $\partial_{x,y,z,w}(G + \lambda F) = 0$  and  $F = 0$  as five equations for  $(x, y, z, w, \lambda)$ . The function  $G$  constrained on the hypersurface reaches an extremum with,  $(x, y, z, w) = (\frac{7}{24}, \frac{7}{24}, \frac{5}{24}, \frac{5}{24})$  and  $\lambda = \frac{1}{8}$ . At this point, we find  $G = \frac{1}{48}$ , which is less than (3.19). Hence, it is not the global maximum. This completes our proof of (3.19) and thus the bounds (3.15).

The inequalities (3.9), (3.14) and (3.15) impose nontrivial unitarity bounds on the transition probabilities  $(X, Y, Z)$ . We present these bounds in Fig. 2, where the allowed region is surrounded by the colored surfaces. First, the conditions of (3.9) restrict  $(X, Y, Z)$  into a cube (yellow color) with each side length equal to  $\frac{1}{2}$ . Second, the inequalities of (3.14) constrain the region through the three green planes, described by the equations  $(X+Y, Y+Z, Z+X) = \frac{2}{3}$ . Finally, Eq. (3.15) further bounds the allowed region through the six blue planes, dictated by the equations  $(2X+Y, 2X+Z, 2Y+Z, 2Y+X, 2Z+X, 2Z+Y) = \frac{25}{24}$ .

## 4 Unitarity Constraints on Flavor Ratios of Astrophysical Neutrinos

As mentioned earlier, the astrophysical neutrinos may originate from different sources. The commonly considered neutrino sources include Pion Sources ( $\pi$ S), Muon-Damped Sources ( $\mu$ DS), and Neutron Beam Sources ( $n$ BS). In this section, we will apply the general unitarity bounds (3.9), (3.14) and (3.15) to derive new constraints on the flavor ratios for different sources of cosmic neutrinos. These general constraints are independent of any experimental input or specific pattern of leptonic mixing.

### 4.1 Pion Sources with Flavor Ratio (1 : 2 : 0)

As mentioned in Sec. 2, the Pion Sources have the initial neutrino flavor ratio equal (1 : 2 : 0). Thus, we can deduce the flavor ratios at the detector as in (2.10),  $T = \frac{1}{3}(2 - 2X - Z)$  and  $S = \frac{1}{3}(1 - Y + Z)$ .

From (3.9) and (3.15), we have,  $-\frac{1}{2} \leq -Y \leq Z - Y \leq Z \leq \frac{1}{2}$  and  $0 \leq 2X + Z \leq \frac{25}{24}$ . Thus, we can deduce

$$\frac{23}{72} \leq T \leq \frac{2}{3}, \quad (4.1a)$$

$$\frac{1}{6} \leq S \leq \frac{1}{2}. \quad (4.1b)$$

Next, we will analyze the unitarity bounds for  $S+T$ ,  $S-T$ ,  $T+2S$ ,  $T+4S$  and  $3S-T$ . We may first compute the combinations of  $T$  and  $S$ ,

$$S + T = 1 - \frac{1}{3}(2X + Y),$$

$$\begin{aligned}
S - T &= -\frac{1}{3} + \frac{1}{3}(2X + 2Z - Y), \\
T + 2S &= \frac{1}{3}(4 - 2X - 2Y + Z), \\
T + 4S &= 2 - \frac{1}{3}(2X + 4Y - 3Z), \\
3S - T &= \frac{1}{3}(1 - 3Y + 2X + 4Z).
\end{aligned} \tag{4.2}$$

From the conditions (3.9) and (3.15), we infer the unitarity bounds on  $S+T$ ,

$$\frac{47}{72} \leq S+T \leq 1. \tag{4.3}$$

The flavor ratio difference  $S-T$  in (4.2) contains  $2X + 2Z - Y$ , which is larger than  $-Y$  and smaller than  $2(X + Z)$ . Thus, from (3.14) and (3.15) we derive,

$$-\frac{1}{2} \leq 2X + 2Z - Y \leq \frac{4}{3}, \tag{4.4}$$

which leads to the bound,

$$-\frac{1}{2} \leq S - T \leq \frac{1}{9}. \tag{4.5}$$

We note that  $T + 2S$  contains the combination  $2X + 2Y - Z$ , which subjects to the same bounds as in Eq. (4.4). Hence, we arrive at

$$\frac{8}{9} \leq T + 2S \leq \frac{3}{2}. \tag{4.6}$$

The upper and lower bounds on  $2X + 4Y - 3Z$  or  $2X + 4Z - 3Y$  are  $\frac{25}{12}$  and  $-\frac{3}{2}$ , respectively, which can be inferred in a similar way to (4.4). Hence, we can deduce

$$\frac{47}{36} \leq T + 4S \leq \frac{5}{2}, \tag{4.7}$$

and

$$-\frac{1}{6} \leq 3S - T \leq \frac{37}{36}. \tag{4.8}$$

We summarize the above unitarity bounds (4.1), (4.3) and (4.5)-(4.8) in Table 1, for Pion Sources with the initial flavor ratio (1:2:0). Combining all these constraints, we identify the allowed region of  $(T, S)$  in Fig. 3, which lies in the shaded area (green color). In Fig. 3, we also present the parameter region (black points) allowed by the current neutrino global fit [11],

$$\begin{aligned}
s_{12}^2 &= (3.08 \pm 0.17) \times 10^{-1}, \\
s_{23}^2 &= (4.37 \pm 0.28) \times 10^{-1}, \\
s_{13}^2 &= (2.34 \pm 0.20) \times 10^{-2}, \\
\delta_D &= (1.39 \pm 0.33)\pi.
\end{aligned} \tag{4.9}$$

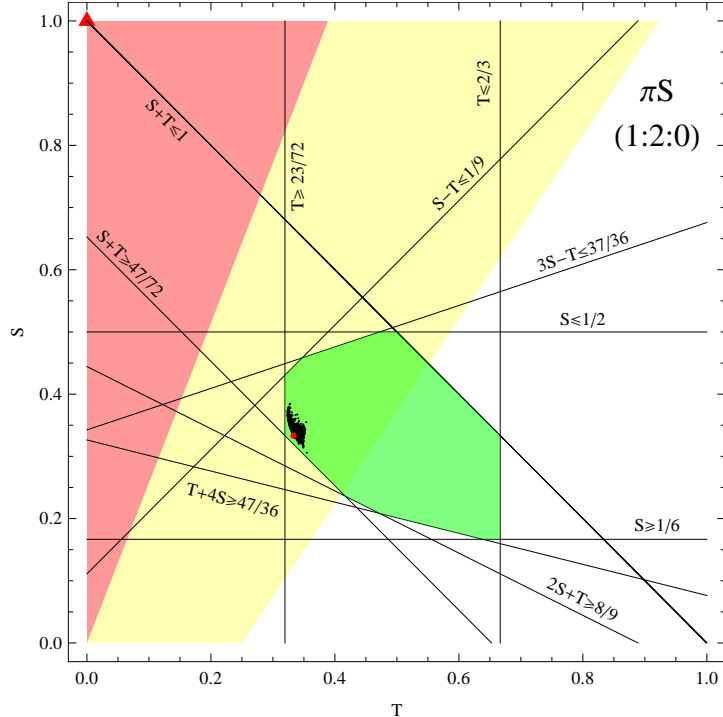


**Figure 3.** Unitarity bounds on the flavor ratios  $(T, S)$ , where we take Pion Sources ( $\pi S$ ) with initial neutrino flavor ratio  $(1:2:0)$ . The black straight lines represent the general bounds (Table 1) derived from the unitarity of the PMNS matrix without experimental input. These bounds are combined to give the allowed region (green area). The dark spot inside the shaded area is a collection of 1000 random points given by the results of a neutrino global fit [11] of the PMNS matrix. The red point nearby the boundary of the green area depicts  $(T, S) = (\frac{1}{3}, \frac{1}{3})$ , and corresponds to a flux ratio of  $(1:1:1)$  at the detector. The shaded red (yellow) region denotes the fit [13] to the three-year IceCube data at 68% C.L. (95% C.L.), with the red-triangle as the best fit.

The global fit (4.9) is for the normal mass-ordering. As we have checked, the global fit for inverted mass-ordering only differs a little, and does not lead to any visible effect in our numerical analyses. Thus, it suffices to use the above fit (4.9) for our present study. Using the global fit (4.9) for the PMNS parameters  $(s_{13}, s_{23}, s_{12}, \delta_D)$  with Gaussian distributions, we have generated 1000 random points in Fig. 3. From this plot, we see that these black points appear nearly as a dark spot in the small region of the  $T - S$  plane, as required by the current neutrino global fit.

Recently, the IceCube collaboration [2] published 37 candidate events after analyzing its three-year data collection (988 days between 2010–2013), with deposited energies within the range of 30–2000 TeV. Among these events 28 are identified as shower events and 7 as muon-track events. IceCube also found [2] that among the 37 recorded events, two events had coincident hits in the IceTop surface array, so they were almost certainly produced in cosmic ray air showers and thus should be subtracted. Although the expected atmospheric back-

**Table 1.** Summary of unitarity constraints on the flavor ratios of astrophysical neutrinos.

$\nu$ Sources	Initial Ratio	Leptonic Unitarity Bounds
$\pi S$	(1 : 2 : 0)	$\frac{23}{72} \leq T \leq \frac{2}{3}, \frac{1}{6} \leq S \leq \frac{1}{2}, \frac{47}{72} \leq T+S \leq 1, -\frac{1}{9} \leq T-S \leq \frac{1}{2}$ $\frac{8}{9} \leq T+2S \leq \frac{3}{2}, \frac{47}{36} \leq T+4S \leq \frac{5}{2}, -\frac{37}{36} \leq T-3S \leq \frac{1}{6}$
$\mu DS$	(0 : 1 : 0)	$\frac{1}{3} \leq T \leq 1, 0 \leq S \leq \frac{1}{2},$ $\frac{1}{2} \leq T+S \leq 1, -\frac{1}{24} \leq T-S \leq 1, \frac{23}{24} \leq 2T+S \leq 2$
$nBS$	(1 : 0 : 0)	$0 \leq T \leq \frac{1}{2}, \frac{1}{3} \leq S \leq 1,$ $\frac{1}{2} \leq T+S \leq 1, -1 \leq T-S \leq \frac{1}{24}, \frac{23}{24} \leq T+2S \leq 2$
Mixture	$(\eta : 1 - \eta : 0)$	$0 \leq (T, S) \leq 1, \frac{1}{2} \leq T+S \leq 1, \max\{2T+S, T+2S\} \geq \frac{23}{24}$

ground rates have some uncertainty (e.g., from high-mass mesons with shorter lifetimes), the energy spectrum, zenith distribution, and muon track to shower ratio of the observed events strongly disagree with the possibility of having these events from purely atmospheric origin, at  $5.7\sigma$  level. Hence, these signals should mainly arise from the astrophysical neutrinos with very large  $L/E$ . After subtracting the two atmospheric muon-like events, the ratio of track events to all signal events is  $7/35 = 0.2$  [2], which indicates that the  $\nu_\mu$  flux ratio  $T$  should be relatively small. It is worth to note that the value of  $T$  does not necessarily equal the ratio of track events to total signal events since the event rate depends on neutrino effective area which varies for different flavor neutrinos [2]. A recent fit of the flux ratios ( $T, S$ ) by using the three-year IceCube data was given in Ref. [13].<sup>2</sup> For the present study, we will compare our general unitarity bounds with the fitted neutrino flux ratios [13], but we keep in mind that a fully realistic and precise fit to the IceCube data should be eventually done by the experimental collaboration itself.

In Fig. 3, we further present the recent fit of flux ratios at 68% C.L. (95% C.L.) [13], as marked by the red (yellow) shaded area, where the red triangle-dot denotes the best fit. As we see, if we take Pion Sources with initial flavor ratio (1 : 2 : 0), the fitted flux ratios of IceCube at 68% C.L. (red region) already lie outside of the unitarity bounds (and the current neutrino global fit [11]), but the IceCube constraints at 95% C.L. (yellow region) are

<sup>2</sup> It is also worth to note that despite corrections from the neutrino effective areas and the atmospheric muon backgrounds, technically translating an event topology to the interacting flavor neutrinos involves complicated analyses. For example, the High Energy Starting Events (HESE) method [14] requires the entering particles being energetic enough and is used to select neutrino-like events by vetoing low energy events in which the earliest light is observed in the outer part of the detector. The complication of such analysis could induce further uncertainty for measuring neutrino fluxes and thus affect the value of flavor composition  $T$ . Clearly, a detailed precise determination of the flux ratios should be eventually done by the experimental collaboration itself. Besides, since the number of signal events is still small, the value of  $T$  is likely to be subject to changes after more upcoming data are analyzed.

still consistent with our unitarity bounds. Under the unitarity bound  $S \leq \frac{1}{2}$  from Eq. (4.1b), we find that the 68% C.L. fit of IceCube (shaded red area in Fig. 3) restricts the  $\nu_\mu$  flux ratio  $T$  to a smaller range,  $T \leq 0.19$ . Thus, if future experiments (including IceCube) could further strengthen this limit and confirm the source as Pion Source, then new physics would be required to explain a small flux ratio  $T$  (significantly below  $23/72 \simeq 0.32$ ), such as sterile neutrinos, neutrino decays, pseudo-Dirac neutrinos, or other exotic effects [10]. The comparison with IceCube in Fig. 3 is instructive. It shows that imposing the unitarity bounds can put nontrivial universal constraints on the flux ratios  $(T, S)$ .

In Fig. 3, the dark spot (consisting of the simulated scattered points) gives the region allowed by the global fit of current neutrino data [11]. We note that it almost saturates the unitarity bound on the lower left-hand-side of  $T$ , i.e., very close to the unitarity bounds  $T \geq 23/72$  and  $T + S \geq 47/72$ . This shows that these two unitarity bounds are very important.

For comparison, we also take a canonical reference point  $(T, S) = (\frac{1}{3}, \frac{1}{3})$ , marked as the red point inside the green area of Fig. 3, which corresponds to the flux ratio of (1:1:1) at the detector.<sup>3</sup> This point was also discussed before for the comparison with fitting the IceCube data [1][13]. Fig. 3 shows that this red point is excluded by the current neutrino global fit, and lies nearby the boundary of our unitarity bounds  $T + S \geq 47/72 \simeq 0.65$  and  $T \geq 23/72 \simeq 0.32$ .

## 4.2 Muon-Damped Sources with Flavor Ratio (0:1:0)

Muon-Damped Sources ( $\mu$ DS) have an initial flavor ratio (0:1:0). Thus, we can infer the flavor ratios at the detector as in (2.11),  $T = 1 - X - Z$  and  $S = Z$ . Using the unitarity conditions (3.9) and (3.14), we deduce the bounds,

$$\frac{1}{3} \leq T \leq 1, \quad 0 \leq S \leq \frac{1}{2}. \quad (4.10)$$

Similar to Sec. 4.1, for the combinations,

$$\begin{aligned} S + T &= 1 - X, \\ 2T + S &= 2 - (2X + Z), \\ T - S &= 1 - (X + 2Z), \end{aligned} \quad (4.11)$$

we derive the following bounds on the flavor ratios,

$$\frac{1}{2} \leq S + T \leq 1,$$

---

<sup>3</sup>For the initial flavor ratio (1:2:0) and the neutrino mixing with  $(\theta_{23}, \theta_{13}) = (\frac{\pi}{4}, 0)$ , the detected flux ratio would be (1:1:1).

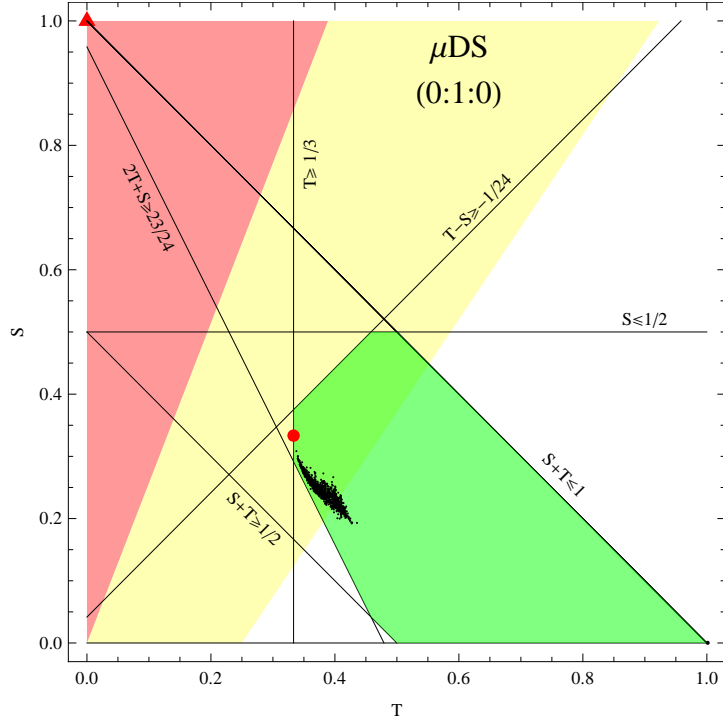


**Figure 4.** Unitarity bounds on the flavor ratios  $(T, S)$ , for Muon-Damped Sources ( $\mu$ DS) with initial neutrino flavor ratio  $(0:1:0)$ . The black straight lines represent the general bounds (Table 1) derived from the unitarity of the PMNS matrix without experimental input. These bounds are combined to give the allowed region (green area). The dark spot inside the shaded area is a collection of 1000 random points given by the result from a neutrino global fit [11] of the PMNS matrix. The red point is defined in the caption of Fig. 3. The shaded red (yellow) region denotes the fit [13] to the three-year IceCube data at 68% C.L. (95% C.L.), with the red-triangle as the best fit.

$$\begin{aligned} \frac{23}{24} &\leq 2T+S \leq 2, \\ -\frac{1}{24} &\leq T-S \leq 1. \end{aligned} \quad (4.12)$$

We summarize the above unitarity bounds in Table 1 for  $\mu$ DS Sources with initial flavor ratio  $(0:1:0)$ . We combine these bounds in Fig. 4, and deduce the allowed region of  $(T, S)$  which is within the shaded green area. The parameter region allowed by the current neutrino global fit is shown by the black points, which nearly form a dark spot, same as in Fig. 3. We note that in this case the dark spot region almost saturate the unitarity bounds on  $T$  from its lower side. This shows that the general bounds  $T \geq \frac{1}{3}$  and  $2T+S \geq \frac{23}{24}$  play an important role here. Furthermore, Fig. 4 shows that, if we take  $\mu$ DS as the neutrino sources with initial flavor composition  $(0:1:0)$ , the current fit [13] to the three-year IceCube data lies outside of the unitarity bound (green region) at 68% C.L. (red region), but is still consistent with the unitarity constraint (green region) at 95% C.L. (yellow region). Here we would note again that a fully realistic fit to the flavor compositions should be done by the experimental collaboration.



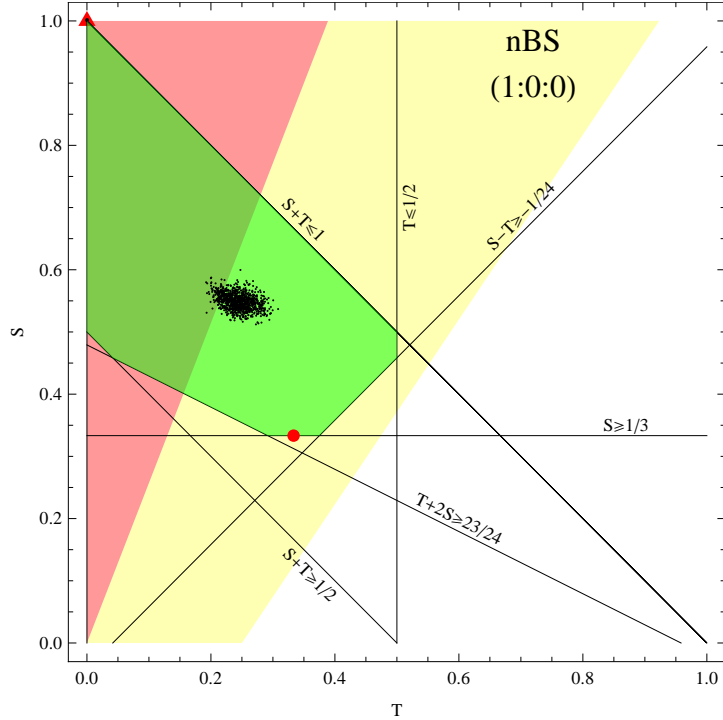


**Figure 5.** Unitarity bounds on the flavor ratios  $(T, S)$ , for Neutron Beam Sources (nBS) with initial flavor ratio  $(1:0:0)$ . The black straight lines represent the general bounds (Table 1) derived from the unitarity of PMNS matrix without experimental input. These bounds are combined to give the allowed region as shown by the shaded green area (including the overlapping part). The dark spot inside the shaded area is a collection of 1000 random points given by the current neutrino global fit [11] of the PMNS matrix. The red point is defined in the caption of Fig. 3. The shaded red (yellow) region denotes the fit [13] to the three-year IceCube data at 68% C.L. (95% C.L.), with the red-triangle as the best fit. This fit is fully consistent with the unitarity bounds and the current global fit [11] of the PMNS matrix.

### 4.3 Neutron Beam Sources with Flavor Ratio $(1:0:0)$

For astrophysical neutrinos from Neutron Beam Sources (nBS) with initial flavor ratio  $(1:0:0)$ , our unitarity analysis is similar to that of Sec. 4.2 for  $\mu$ DS with the initial flavor ratio  $(0:1:0)$ .

In the case of nBS sources, we have  $T = Z$  and  $S = 1 - Z - Y$ . Thus, we derive the combinations  $S + T$ ,  $T + 2S$ , and  $S - T$  in terms of  $(X, Y, Z)$ ,

$$\begin{aligned}
 S + T &= 1 - Y, \\
 T + 2S &= 2 - (2Y + Z), \\
 S - T &= 1 - (Y + 2Z).
 \end{aligned}
 \tag{4.13}$$

In parallel to Sec. 4.2, we derive unitarity bounds on the flavor ratios,

$$0 \leq T \leq \frac{1}{2}, \quad \frac{1}{3} \leq S \leq 1, \quad (4.14)$$

and their combinations above,

$$\begin{aligned} \frac{1}{2} &\leq S+T \leq 1, \\ \frac{23}{24} &\leq T+2S \leq 2, \\ -\frac{1}{24} &\leq S-T \leq 1. \end{aligned} \quad (4.15)$$

We summarize these bounds into Table 1, and present their combined bounds (shaded green area) in Fig. 5. From this plot, it is interesting to see that the current fit [13] to the IceCube data is compatible with the unitarity bounds (green area) for the nBS sources already at 68% C.L. (red area), because of the large overlapping region. Furthermore, at 95% C.L. (yellow area) the fit [13] is fully consistent with the unitarity bounds, as well as the current neutrino global fit [11] (as represented by the black points in the dark spot region). Comparing Fig. 5 with Fig. 3-4, we see that the fit [13] tends to favor the origin of astrophysical neutrinos to contain a sizable fraction of the nBS sources with initial flavor composition (1:0:0). In the next subsection, we will further analyze a mixed source of the three types, with a generic flux ratio ( $\eta : 1-\eta : 0$ ).

#### 4.4 Mixed Sources with Flavor Ratio ( $\eta : 1-\eta : 0$ )

In general, we can consider a mixed neutrino source of the three types above, where the  $\nu_\tau$  neutrinos are absent. So, this general source has the initial flavor ratio ( $\eta : 1-\eta : 0$ ) with  $\eta \in [0, 1]$ . In this notation, Pion Sources correspond to  $\eta = \frac{1}{3}$ , Neutron Beam Sources to  $\eta = 1$ , and Muon-Damped Sources to  $\eta = 0$ . Thus, for the general case we have the flavor ratios,

$$T = \eta Z + (1-\eta)(1-X-Z), \quad (4.16a)$$

$$S = \eta(1-Z-Y) + (1-\eta)Z. \quad (4.16b)$$

As we noted below Eq. (2.9), under the exchange  $\nu_e \leftrightarrow \nu_\mu$ , we have,  $(X, Z) \leftrightarrow (Y, Z)$  and  $\eta \leftrightarrow (1-\eta)$ . Then, from (4.16), we see that this exchange leads to  $S \leftrightarrow T$ . This property will also ensure the unitarity bound (the shaded region with light blue color) in Fig. 6 to be symmetric with respect to the line  $S = T$ .

For a given  $\eta$  and  $T$ , we may view (4.16a) as a straight line in the  $X-Z$  plane of Fig. 2,

$$Z = -\frac{1-\eta}{1-2\eta}X - \frac{T-(1-\eta)}{1-2\eta}, \quad (4.17)$$

where the slope is fully determined by  $\eta$ , and  $T$  only affects the intercept at  $X = 0$ . In the  $XYZ$  coordinate frame of Fig. 2, Eq. (4.17) describes a plane which is perpendicular to the  $X-Z$  plane and intersects with it at the line given by (4.17). It is clear that for  $\eta \in [0, 1/2)$  and as  $T$  decreases, the plane (4.17) increases its intercept at  $Z$  axis in Fig. 2. If  $T$  decreases to a value such that this plane no longer intersects the space surrounded by the colored surfaces in Fig. 2, i.e., every point in this plane violates the unitarity bound, then this value of  $T$  is disallowed by the unitarity. Thus, we can derive a lower bound on  $T$  by moving the plane (4.17) to the “critical position” where it is just going to fully leave the colored surfaces (unitarity bounds) of Fig. 2.

For  $\eta \in [0, 1/3]$ , the slope of the line (4.17) is restricted within  $[-2, -1]$ . So, from Fig. 2, its critical position should be the point B in the  $X-Z$  plane, and has the coordinates  $(X, Z) = (3/8, 7/24)$ . At the point B, Eq. (4.16a) gives,  $T[B] = (8 - \eta)/24$ . This gives the lower bound  $T \geq (8 - \eta)/24$  for  $\eta \in [0, 1/3]$ . Similarly, for  $\eta \in [1/3, 1/2]$ , the slope of (4.17) is within  $(-\infty, -2]$ . We find that the critical position of (4.17) should be the point A and has the coordinates  $(X, Z) = (1/2, 1/24)$ . Thus, we compute the value of  $T$  at this point,  $T[A] = (11 - 10\eta)/24$ . Hence, we deduce the unitarity bound  $T \geq (11 - 10\eta)/24$  for  $\eta \in [1/3, 1/2]$ . Finally, for  $\eta \in [1/2, 1]$ , the slope of (4.17) is within  $[0, +\infty)$ . In this case, the intercept of (4.17) is the sum of two parts,  $(1 - \eta)/(1 - 2\eta) \in (-\infty, 0]$  and  $T/(2\eta - 1) > 0$ . Thus, decreasing  $T$  will reduce the intercept and move the line (4.17) downwards, which will reach a critical position at the point  $(X, Z) = (1/2, 0)$ . At this point we find the corresponding lower bound,  $T \geq (1 - \eta)/2$ . Combining these bounds, we arrive at

$$\begin{aligned} T &\geq \frac{1}{24}(8 - \eta), & \text{for } \eta \in [0, \frac{1}{3}], \\ T &\geq \frac{1}{24}(11 - 10\eta), & \text{for } \eta \in [\frac{1}{3}, \frac{1}{2}], \\ T &\geq \frac{1}{2}(1 - \eta), & \text{for } \eta \in [\frac{1}{2}, 1]. \end{aligned} \quad (4.18)$$

From Eq. (4.18), we note that for  $\eta \leq \frac{1}{2}$ ,  $T \geq \frac{1}{4}$  always holds; and only when  $\eta > \frac{1}{2}$ , we have  $T < \frac{1}{4}$ . Hence, even if we do not know which types of cosmic neutrino sources are invoked, from the IceCube measurement we can extract important information about the initial flavor composition. For instance, if the measured  $T$  value by IceCube confirms  $T < \frac{1}{4}$  and there is no  $\nu_\tau$  source, then  $\eta > \frac{1}{2}$  has to hold. Hence, we can infer that more  $\nu_e$  neutrinos than  $\nu_\mu$  neutrinos exist in the initial flavor composition of cosmic neutrinos.

Next, we further analyze the unitarity constraints on  $T+S$ . From (4.16), we have

$$T + S = 1 - [\eta Y + (1 - \eta)X]. \quad (4.19)$$

From Eqs. (2.4) and (3.9), we have  $0 \leq (X, Y) \leq \frac{1}{2}$ . Thus, for  $\eta \in [0, 1]$ , we can deduce

$$\frac{1}{2} \leq T + S \leq 1, \quad (4.20)$$

where the lower bound is reached for  $X = Y = \frac{1}{2}$  and the upper bound is saturated if  $X = Y = 0$ .

With the formulas from Eq. (4.16), we deduce the combinations  $2T+S$  and  $T+2S$  as follows,

$$\begin{aligned} 2T+S &= (2-\eta) - [2(1-\eta)X + \eta Y + (1-2\eta)Z] \\ &= (2-\eta) - [\eta(2X+Y) + (1-2\eta)(2X+Z)], \end{aligned} \quad (4.21a)$$

$$\begin{aligned} T+2S &= (1+\eta) - [(1-\eta)X + 2\eta Y - (1-2\eta)Z] \\ &= (1+\eta) - [(1-\eta)(2Y+X) + (2\eta-1)(2Y+Z)]. \end{aligned} \quad (4.21b)$$

As a consistency check, we note that the above formula for  $T+2S$  can be inferred from  $2T+S$  by the exchanges of  $(X, Z) \leftrightarrow (Y, Z)$  and  $\eta \leftrightarrow (1-\eta)$ , because these exchanges lead to  $S \leftrightarrow T$  and thus  $(2T+S) \leftrightarrow (T+2S)$ .

Using the conditions (3.15), we derive the following lower bounds from (4.21a) with  $\eta \leq \frac{1}{2}$  and from (4.21b) with  $\eta \geq \frac{1}{2}$ , respectively,

$$\begin{aligned} 2T+S &\geq \frac{23+\eta}{24}, \quad \text{for } \eta \in [0, \frac{1}{2}], \\ T+2S &\geq 1 - \frac{\eta}{24}, \quad \text{for } \eta \in [\frac{1}{2}, 1]. \end{aligned} \quad (4.22)$$

For any  $\eta \in [0, 1]$ , we see at least one of the combinations  $2T+S$  and  $T+2S$  is larger than  $\frac{23}{24}$ . Hence, we have the combined lower bound,

$$\max\{2T+S, 2S+T\} \geq \frac{23}{24}. \quad (4.23)$$

From the above analysis, we summarize the unitarity constraints (4.20) and (4.23) for the generic flavor ratio ( $\eta : 1-\eta : 0$ ) in Table 1, which hold for any  $\eta \in [0, 1]$ . For demonstration, we further present these general bounds in Fig. 6, where we derive the combined unitarity bound in the  $T-S$  plane, as depicted by the green area (including the overlapping part). As we expected earlier, this unitarity bound (green region) is symmetric respect to the line  $S = T$ . We note that this general bound holds for any  $\eta$  value and is weaker than the bounds of Figs. 3–5 (which correspond to specific  $\eta$  values). Actually, each bounded area in Figs. 3–5 is contained as a certain part of the allowed region in Fig. 6.

From the general bounds in Fig. 6, we see that even though the type of the cosmic neutrino sources is unknown a priori, we can still deduce nontrivial unitarity constraints on the flux ratios  $T$  and  $S$ . This means that for any source among ( $\pi\text{S}, \mu\text{DS}, n\text{BS}$ ) or their general mixture in its initial flavor composition, the flux ratios ( $T, S$ ) must lie in the shaded green region of Fig. 6. Otherwise, the unitarity bounds are violated, which would

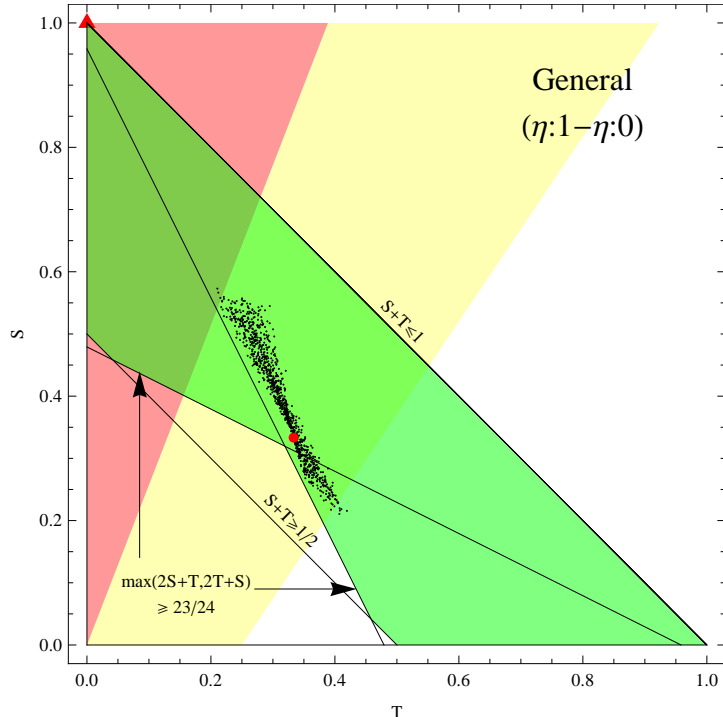


**Figure 6.** Unitarity bounds on the flavor ratios ( $T$ ,  $S$ ), for a generic mixture of three types of sources ( $\pi S$ ,  $\mu DS$ ,  $nBS$ ) with initial flavor ratio  $(\eta : 1-\eta : 0)$  and  $\eta \in [0, 1]$ . The black straight lines represent the general bounds (Table 1) derived from the unitarity of PMNS matrix without experimental input. These bounds are combined to give the allowed green region (including the overlapping part). The dark spot inside the shaded area collects 2000 random points given by the current neutrino global fit of PMNS matrix and with a scan of  $\eta \in [0, 1]$ . The red point is defined in the caption of Fig. 3. The shaded red (yellow) region denotes the fit [13] to the three-year IceCube data at 68% C.L. (95% C.L.), with the red-triangle as the best fit. This fit is consistent with the unitarity bounds.

require proper underlying new physics. For a comparison, we present the recent fit [13] to the three-year IceCube data in the same plot, shown as the shaded red (yellow) area at 68% C.L. (95% C.L.). The plots in Fig. 5–6 also suggest that more precise measurements of the  $\nu_e$  flux ratio  $S$  will be important for pinning down the initial flavor composition in the source.

## 5 Conclusions

Observations of ultra-high-energy astrophysical neutrinos at IceCube [1, 2] have marked the exciting start of neutrino astronomy. This may eventually help astronomers to map individual sources of astrophysical neutrinos in the sky, and thus paint a picture of the universe by means of neutrino telescopes.

In this work, we made use of the unitarity of leptonic PMNS mixing matrix, and systematically derived unitarity constraints on the flavor composition of astrophysical neutrinos, in

comparison with the recent fit [13] to the three-year IceCube data [2] and the current neutrino global fit [11, 12]. In Section 2, using the leptonic unitarity triangles (LUTs) [8], we formulated the flavor transition probabilities of astrophysical neutrinos in terms of the geometrical parameters of the LUTs, as given in Eqs. (2.3)–(2.6). Then, we expressed the  $\nu_\mu$  and  $\nu_e$  flux ratios ( $T$ ,  $S$ ) by the LUT parameters in Eqs. (2.10)–(2.13) for different neutrino sources and their mixture. In Section 3, we quantitatively derived nontrivial unitarity bounds on the transition probabilities of cosmic neutrinos by using the geometrical conditions (such as the triangular inequalities). These are presented in Eqs. (3.9)–(3.11) and Eqs. (3.14)–(3.15), as well as Figs. 1–2. These and other new bounds we derived generally hold for three flavor neutrinos, independent of any experimental input or the pattern of leptonic mixing.

In Section 4, we applied these generic unitarity bounds to impose constraints on the flux ratios ( $T$ ,  $S$ ) for three types of the neutrino sources ( $\pi$ S,  $\mu$ DS,  $n$ BS) and their general mixture. These unitarity constraints are summarized in Table 1. In Figs. 3–6, we compared these constraints with the IceCube data [2], as well as the current neutrino global fit [11]. With the cosmic neutrino flux ratios extracted from the recent fit [13] to the three-year IceCube data [2], we found that the  $\pi$ S or  $\mu$ DS sources would be disfavored by unitarity bounds at 68% C.L., but still consistent with the unitarity at 95% C.L., as shown in Figs. 3–4. If the  $\pi$ S or  $\mu$ DS sources are the real origin of the observed astrophysical neutrinos, a further confirmation of the IceCube data away from the unitarity bounds would suggest either a misidentification of certain tracks as showers, or a misunderstanding of the potential background events, or the existence of underlying new physics beyond the standard model. In addition, for neutrino sources such as the  $n$ BS or the mixed sources, we revealed that the recent IceCube fit [13] is consistent with our unitarity bounds (as well as the current neutrino global fit) at both 68% C.L. and 95% C.L., as shown in Figs. 5–6. Even without specifying the type of sources, the suggested flavor ratio (1:1:1) at the detector is within and very close to our unitarity bound, and is compatible with the IceCube data at 95% C.L. (Fig. 6).<sup>4</sup>

Finally, in Section 4.4, we proved that for any sources without  $\nu_\tau$  neutrinos (such as  $\pi$ S,  $\mu$ DS,  $n$ BS, or their mixture), a detected  $\nu_\mu$  flux ratio  $T < 1/4$  will require the initial flavor composition with more  $\nu_e$  neutrinos than  $\nu_\mu$  neutrinos.

## Acknowledgements

We thank John R. Ellis, Eligio Lisi, Sergio Palomares-Ruiz and Xiangyang Yu for useful discussions. XJX and HJH were supported by Chinese NSF (Grant No. 11275101 and 11135003)

<sup>4</sup>As we commented in footnote-2, the complication of uncertainties of the experimental HESE analysis may cause possible mis-reconstruction of events at the topology level. Hence, a fully realistic and reliable fit to the IceCube data should be done by the experimental collaboration itself, which will put any conclusion on a firmer ground.

and National Basic Research Program (No. 2010CB833000). WR was supported by the Max Planck Society in the project MANITOP.

## References

- [1] M. G. Aartsen *et al.*, [IceCube Collaboration], *Science* **342** (2013) 1242856 [arXiv:1311.5238 [astro-ph.HE]].
- [2] M. G. Aartsen *et al.*, [IceCube Collaboration], *Phys. Rev. Lett.* **113** (2014) 101101 [arXiv:1405.5303 [astro-ph.HE]]; and C. Kopfer, presentation at the XLIX Rencontres de Moriond EW, March 15-22, 2014, Moriond, La Thuile, Italy.
- [3] W. Winter, *Adv. High Energy Phys.* **2012** (2012) 586413 [arXiv:1201.5462 [astro-ph.HE]]; L. A. Anchordoqui *et al.*, *Journal of High Energy Astrophysics* **1-2** (2014) 1 [arXiv:1312.6587 [astro-ph.HE]].
- [4] KM3NeT Collaboration, <http://km3net.org>; P. Gorham *et al.*, [ANITA collaboration], *Phys. Rev. Lett.* **103** (2009) 051103; Pierre Auger Collaboration, *Phys. Rev. D* **79** (2009) 102001; P. Allison *et al.*, *Nucl. Instrument & Method A* **604** (2009) S64.
- [5] E.g., J. G. Learned and S. Pakvasa, *Astropart. Phys.* **3** (1995) 267 [hep-ph/9405296, hep-ph/9408296]; L. Bento, P. Keranen and J. Maalampi, *Phys. Lett. B* **476** (2000) 205 [hep-ph/9912240]; H. Athar, M. Jezabek and O. Yasuda, *Phys. Rev. D* **62** (2000) 103007 [hep-ph/0005104]; G. Barenboim and C. Quigg, *Phys. Rev. D* **67** (2003) 073024 [hep-ph/0301220]; J. F. Beacom, N. F. Bell, D. Hooper, S. Pakvasa, and T. J. Weiler, *Phys. Rev. D* **68** (2003) 093005 [Erratum-ibid. *D* **72** (2005) 019901] [hep-ph/0307025]; P. D. Serpico and M. Kachelriess, *Phys. Rev. Lett.* **94** (2005) 211102 [hep-ph/0502088]; W. Winter, *Phys. Rev. D* **74** (2006) 033015 [hep-ph/0604191]; Z. Z. Xing, *Phys. Rev. D* **74** (2006) 013009 [hep-ph/0605219]; W. Rodejohann, *JCAP* **0701** (2007) 029 [hep-ph/0612047]; D. Meloni and T. Ohlsson, *Phys. Rev. D* **75** (2007) 125017 [hep-ph/0612279]; P. Lipari, M. Lusignoli, and D. Meloni, *Phys. Rev. D* **75** (2007) 123005 [arXiv:0704.0718 [astro-ph]]; K. Blum, Y. Nir, and E. Waxman, arXiv:0706.2070 [hep-ph]; S. Pakvasa, W. Rodejohann, and T. J. Weiler, *JHEP* **0802** (2008) 005 [arXiv:0711.4517 [hep-ph]]; S. Choubey, V. Niro and W. Rodejohann, *Phys. Rev. D* **77** (2008) 113006 [arXiv:0803.0423 [hep-ph]]; M. Maltoni and W. Winter, *JHEP* **07** (2008) 064 [arXiv:0803.2050 [hep-ph]]; Z. Z. Xing and S. Zhou, *Phys. Lett. B* **666** (2008) 166 [arXiv:0804.3512 [hep-ph]]; A. Esmaili and Y. Farzan, *Nucl. Phys. B* **821** (2009) 197 [arXiv:0905.0259 [hep-ph]]; A. Bhattacharya, R. Gandhi, W. Rodejohann, and A. Watanabe, *JCAP* **1110** (2011) 017 [arXiv:1108.3163 [astro-ph.HE]]; L. Fu, C. M. Ho, and T. J. Weiler, *Phys. Lett. B* **718** (2012) 558 [arXiv:1209.5382 [hep-ph]]; K. C. Lai, G. L. Lin, T. C. Liu, *Phys. Rev. D* **89** (2014) 033002 [arXiv:1308.1828 [hep-ph]]; L. Fu and C. M. Ho, arXiv:1407.1090 [hep-ph]; V. Barger, L. Fu, J. G. Learned, D. Marfatia, S. Pakvasa, and T. J. Weiler, arXiv:1407.3255 [astro-ph.HE] and references therein.
- [6] Z. Z. Xing and S. Zhou, *Phys. Rev. D* **74** (2006) 013010 [astro-ph/0603781]; S. Choubey and W. Rodejohann, *Phys. Rev. D* **80** (2009) 113006 [arXiv:0909.1219].
- [7] B. Pontecorvo, *Zh. Eksp. Teor. Fiz.* **33** (1957) 549; **34** (1958) 247; Z. Maki, M. Nakagawa, and S. Sakata, *Prog. Theor. Phys.* **28** (1962) 870.
- [8] H. J. He and X. J. Xu, *Phys. Rev. D* **89** (2014) 073002 [arXiv:1311.4496].
- [9] For a partial list of earlier studies, *e.g.*, H. Fritzsch and Z. Z. Xing, *Prog. Part. Nucl. Phys.* **45** (2000) 1 [arXiv:hep-ph/9912358]; J. A. Aguilar-Saavedra and G. C. Branco, *Phys. Rev. D* **62** (2000) 096009 [hep-ph/0007025]; J. Sato, *Nucl. Instrum. Meth. A* **472** (2001) 434 [arXiv:hep-ph/0008056]; Y. Farzan and A. Yu. Smirnov, *Phys. Rev. D* **65** (2002) 113001 [arXiv:hep-ph/0201105]; H. Zhang and Z. Z. Xing, *Eur. Phys. J. C* **41** (2005) 143 [arXiv:hep-ph/0411183]; Y. Koide, arXiv:hep-ph/0502054; S. Antusch, C. Biggio, E.

- Fernandez-Martinez, M. B. Gavela, and J. Lopez-Pavon, JHEP **0610** (2006) 084 [arXiv:hep-ph/0607020]; J. D. Bjorken, P. F. Harrison and W. G. Scott, Phys. Rev. D **74** (2006) 073012 [hep-ph/0511201]; G. Ahuja and M. Gupta, Phys. Rev. D **77** (2008) 057301 [hep-ph/0702129]; A. Dueck, S. Petcov, and W. Rodejohann, Phys. Rev. D **82** (2010) 013005 [arXiv:1006.0227]; S. Luo, Phys. Rev. D **85** (2012) 013006 [arXiv:1109.4260]; P. S. BhupalDev and R. N. Mohapatra, Phys. Rev. D **81** (2010) 013001 [arXiv:0910.3924]; P. S. BhupalDev, C. H. Lee, and R. N. Mohapatra, Phys. Rev. D **88** (2013) 093010 [arXiv:1309.0774]; and references therein.
- [10] J. F. Beacom, N. F. Bell, D. Hooper, S. Pakvasa, and T. J. Weiler, Phys. Rev. Lett. **90** (2003) 181301 [hep-ph/0211305]; J. F. Beacom, N. F. Bell, D. Hooper, S. Pakvasa, and T. J. Weiler, Phys. Rev. D **69** (2004) 017303 [hep-ph/0309267]; A. Bhattacharya, S. Choubey, R. Gandhi, and A. Watanabe, Phys. Lett. B **690** (2010) 42 [arXiv:0910.4396 [hep-ph]]; P. Mehta and W. Winter, JCAP **1103** (2011) 041 [arXiv: 1101.2673 [hep-ph]]; P. Baerwald, M. Bustamante, and W. Winter, JCAP **1210** (2012) 020 [arXiv:1208.4600 [astro-ph.CO]]; A. Bhattacharya, R. Gandhi, W. Rodejohann, and A. Watanabe, arXiv:1209.2422 [hep-ph]; K. N. Abazajiana *et al.*, arXiv:1204.5379 [hep-ph]; and references therein.
- [11] F. Capozzi, G. L. Fogli, E. Lisi, A. Marrone, D. Montanino, and A. Palazzo, Phys. Rev. D **89** (2014) 093018 [arXiv:1312.2878v2 [hep-ph]].
- [12] D. V. Forero, M. Tortola, J. W. F. Valle, arXiv:1405.7540 [hep-ph].
- [13] O. Mena, S. Palomares-Ruiz, and A. C. Vincent, Phys. Rev. Lett. **113** (2014) 091103 [arXiv: 1404.0017 [astro-ph.HE]]. For an updated fit with the 3-year IceCube data, S. Palomares-Ruiz, talk in Munich, June 13, 2014, “On the flavor composition of the high-energy neutrinos in IceCube”, ([http://www.t30d.ph.tum.de/JAPS/Sergio\\_PalomaresRuiz\\_IceCube.pdf](http://www.t30d.ph.tum.de/JAPS/Sergio_PalomaresRuiz_IceCube.pdf)).
- [14] M. G. Aartsen *et al.*, [IceCube Collaboration], “The IceCube Neutrino Observatory”, Part I-II, arXiv:1309.6979 [astro-ph.HE] and arXiv:1309.7003 [astro-ph.HE], the 33rd International Cosmic Ray Conference, Rio de Janeiro, 2013.
- [15] E.g., C. Y. Chen, P. S. BhupalDev, and A. Soni, Phys. Rev. D **89** (2014) 033012 [arXiv:1309.1764 [hep-ph]]; D. Fargion and P. Paggi, Nucl. Instrum. Meth. A **753** (2014) 9 [arXiv:1310.3543 [astro-ph.HE]]; D. Fargion, arXiv:1404.5914 [astro-ph.HE]; and references therein.
- [16] C. Jarlskog, Phys. Rev. Lett. **55** (1985) 1039.